Physica Scripta

INCLUSIVE PUBLISHING TRUSTED SCIENCE

PURPOSE-LED PUBLISHING™

PAPER • **OPEN ACCESS**

Investigation of radiation shielding properties of CeO_2 thin films prepared at different molarities

To cite this article: İmran Kanmaz *et al* 2025 *Phys. Scr.* **100** 035945

View the article online for updates and enhancements.

You may also like

- A wideband high gain conformal self-decoupled multiport antenna for 5G millimeter wave communications
Priyanka Das and Surajit Kundu
- Some properties of hyperbolic Yamabe solitons
Adara M Blaga and Cihan Özgür
- n-Si/p-BaO/p-SiO_2 heterojunctions designed as negative capacitance and negative conductance sources, 6G technology frequency stabilizers, and current rectifiers
M Y Al-Harbi, A F Qasrawi and Seham R Alharbi

This content was downloaded from IP address 161.9.200.62 on 13/04/2026 at 14:48

Physica Scripta

PAPER

Investigation of radiation shielding properties of CeO_2 thin films prepared at different molarities

İmran Kanmaz[1,2,3,*], **Oğuz Kağan Köksal**[3,4], **Gökhan Apaydin**[1,3], **Murat Tomakin**[2] and **Erhan Cengiz**[3,5]

[1] Department of Physics, Karadeniz Technical University, 53100 Trabzon, Türkiye
[2] Department of Physics, Recep Tayyip Erdogan University, 53100 Rize, Türkiye
[3] Gamma and x-Ray Applications Research Group (GXARG), Department of Physics,Karadeniz Technical University, 61080, Trabzon, Türkiye
[4] Gölbaşı Vocational High School Department of Electricity and Energy 02500 Adıyaman, Türkiye
[5] Department of Fundamental Science, Alanya Alaaddin Keykubat University, 07425, Antalya, Türkiye
[*] Author to whom any correspondence should be addressed.

E-mail: imrankanmaz@ktu.edu.tr, okoksal@adiyaman.edu.tr, gapaydin@ktu.edu.tr, murat.tomakin@erdogan.edu.tr and erhan.cengiz@alanya.edu.tr

Keywords: CeO_2, thin film, radiation shielding, Sol-Gel

OPEN ACCESS

RECEIVED
16 December 2024

REVISED
23 January 2025

ACCEPTED FOR PUBLICATION
6 February 2025

PUBLISHED
17 February 2025

Original content from this work may be used under the terms of the Creative Commons Attribution 4.0 licence.

Any further distribution of this work must maintain attribution to the author(s) and the title of the work, journal citation and DOI.

Abstract

In this study, CeO_2 thin films were produced using the spin coting method, which is one of the sol–gel methods, in six different molarities. X-ray diffraction (XRD) patterns revealed the characteristic peaks of the films, while Field Emission Scanning Electron Microscopy (FESEM) confirmed their homogeneous structure. Then, radiation shielding parameters like linear absorption coefficient (LAC), mass absorption coefficient (MAC), tent value layer (TVL), mean free path (MFP), and half value layer (HVL) were thoroughly examined. The results showed that increasing molarity had a significant effect on the thickness values of thin films and the absorption parameters were found to improve with increasing molarity. Both LAC and MAC values decrease as the energy level increases, but the increase in CeO_2 molarity leads to a strong increase on these coefficients. The HVL value was also found to be 0.42 cm at the lowest energy of 14.957 keV and to be around 10 cm at the greatest energy of 59.543 keV (0.05 M). When the radiation energy applied to the material was raised from 14.957 keV to 59.543 keV, it was found that the MFP values of 0.05 M CeO_2 thin films grew gradually from 0.61 cm to 14.51 cm. High energy radiation of 59.543 keV and a low density (0.05 M) medium resulted in peak TVL values of 33.423 cm, allowing the radiation to pass through the material with minimal interaction.

1. Introduction

As a result of the advancement of technology and its widespread use in industry, people are exposed to more ionizing radiation [1]. Scientists have focused on various studies to protect people from the harmful effects of radiation. One of these studies is on the use of thin film technology as a radiation shielding. The use of thin films as radiation shields is not only important for human health but also for technological devices [2–4]. Dense materials such as lead and concrete are generally used as radiation shielding [5]. However, the low optical transmittance of lead poses a major obstacle to its use in some applications of technology. For example, since lead is used in the production of glasses used for radiation protection, the optical transmittance of these glasses is quite low. This reduces the quality of vision when using these glasses. In the literature research, it has been observed that optical transmittance decreases as the lead doping ratio increases in lead doped thin films [6, 7]. Fabrication of thin films with high optical transmittance and radiation absorption capacity is important for human health and some technological applications. In this study, the radiation absorption effects of CeO_2 thin films produced in six different thicknesses were examined in detail depending on five different energies. CeO_2

© 2025 The Author(s). Published by IOP Publishing Ltd

thin films stand out as a fascinating material with numerous applications. CeO_2 possesses exceptional properties, including high atomic number, a wide band gap, high dielectric constant, high chemical stability, remarkable mechanical strength, excellent lattice compatibility, a good refractive index for optical applications and transparency in the visible and near-infrared spectral regions [8–10]. The high atomic number and density of these elements contribute significantly to their ability to attenuate and absorb ionizing radiation [11]. Considering these properties, it shows that CeO_2 thin films can be preferred as radiation shields. When literature studies are examined, it is seen that although studies investigating CeO_2 thin films as radiation shields are encountered, the studies conducted are limited. In addition, this study differs from other studies in the literature in terms of preparing thin films produced at different molarities in various thicknesses and examining the absorption properties depending on thickness and energy by exposing these films to radiation at six different energies. In recent years, CeO_2 thin films have been successfully utilized in various technological applications, including catalytic [12], electrochemical [13], optical [14], electrical [15], gas sensor [16], corrosion-resistant applications [17, 18] and UV-blocking filters [19]. In this study, homogeneous and economical films were obtained by using the spin coating method for the fabrication of CeO_2 thin films. One of the reasons for using the spin coating technique is that it is very easy to apply and can be obtained at a relatively low cost. The physical properties of the films obtained depend on thermal annealing and thermal annealing time [20–22]. However, various coating parameters such as coating speed, coating time and molarity of the precursor solution also play a role in the physical properties of thin films during coating [23, 24]. In this study, the radiation absorption parameters of CeO_2 thin films with six different thicknesses and five different energies were investigated in detail. Considering the large number of studies conducted in this field [25–27], it is thought that this study will make important contributions to the literature.

2. Experimental section

2.1. Methodology

The system is called a narrow geometry Am-241radioisotope source attenuation geometry. The Americium-241 radioactive annular source was selected because to its compatibility with secondary targets, ability to facilitate non-destructive excitation, independence from a power source, and capacity to generate an adequate quantity of gamma rays. Photons from the Am-241 source, which produces photons with an energy of 59.5 keV, are sent to the detector without a sample. The number of photons is recorded as a blank count. Then, the sample is added, and the same process is performed. This time, the photons passing through the sample are recorded. According to the Lambeer-Beert law, calculations are made with these photon numbers, and the mass absorption coefficient is calculated. Taking the sample density into account, the linear absorption coefficient and the mean free path, half-value thickness and tenth value thickness parameters derived from here are calculated.

2.2. Fabrication and characterization of CeO_2 thin films

CeO_2 thin films were coated on the c-Si surface by spin coating method. Cerium (III) chloride heptahydrate ($CeCl_3{\cdot}7H_2O$, Sigma-Aldrich) with a purity of 99% was used as the source of cerium, while ethyl alcohol was preferred as the solvent. 0.2 M citric acid monohydrate (Merck, 99.7%) was added to the solution, stirred in a magnetic stirrer for 30 min and aged for 24 h. To increase the adhesion of thin films, 75 μl of triethanolamine (97%) was added to 5 ml of solution and mixed at 50 °C for half an hour. The coating was carried out CZ-Si p-type wafers with a thickness of 725 μm and a size of 1 cm × 1 cm. The wafers was cleaned for 5 min in an ultrasonic bath using ethyl alcohol and deionized water. Then the natural SiO_2 layer was removed with HF (1:10) solution. The coating was carried out at a speed of 6000 rpm for 10 seconds so that the solution spreads over the surface and dried at 200 °C for 5 min. XRD patterns were obtained using a Rigaku Smartlab diffractometer with CuKα radiation ($\lambda = 1.5408$ Å) to examine the crystal structures of the thin films. FESEM images were performed with the Zeiss Sigma 300 model to examine the surface morphology of thin films.

2.3. Gamma ray attenuation measurements

The experimental configuration is illustrated in figure 1. It encompasses the secondary source, the primary source (Am-241), the absorber, and the detecting apparatus. The secondary source beam strikes the Am target, while the absorber collects the emitted beam from the Am target. A collimated Ultra-LEGe (Ortec) detector was used to measure the transmitted gamma rays. The detector exhibits a relative yield of 25% at 1.33 MeV and a resolution of 1.85 keV at the same energy level. The output preamplifier, capable of rejecting pulse pile-ups, transmitted signals to a multichannel analyser linked to a personal computer equipped with appropriate software for data collection and peak analysis. A peak fitting program conducted the fitting and deconvolution procedures. Radiation absorption measurements at different energies were performed to determine the shielding parameters of thin films.

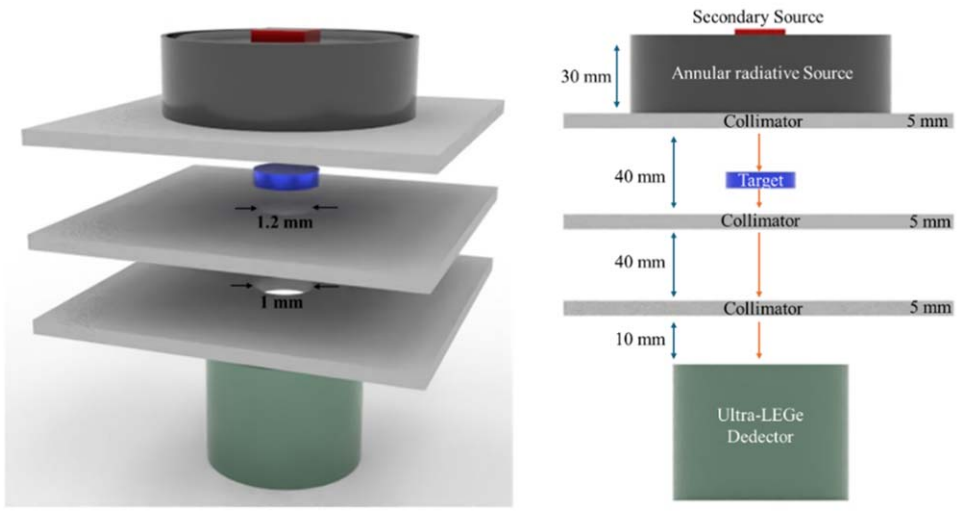

Figure 1. The schematic configuration of the measurement system.

2.4. Calculations

The attenuation coefficients were determined using the Lambert–Beer equation for Cerium dioxide thin films at various molarity levels, employing prior analytical results [28];

$$I = I_0 e^{-\mu x} = I_0 e^{-\left(\frac{\mu}{\rho}\right)d} \tag{1}$$

I_0 represents the incident beam directed towards the detector from the x-ray source in the absence of any sample. The beam is conveyed from the sample to the detector. d represents the mass per unit area (g/cm^2), whereas μ/ρ denotes the mass attenuation coefficient (cm^2/g) [29];

$$\left(\frac{\mu}{\rho}\right)_c = \sum_i W_i(\mu/\rho)_i \tag{2}$$

where Wi represents the weight fraction and the mass attenuation coefficient of the ith constituent element, respectively. The weight fraction of a chemical substance is expressed by equation (3) [30];

$$W_i = \frac{n_i A_i}{\sum_i n_i A_i} \tag{3}$$

The atomic weight of the ith element is denoted as A_i, while the quantity of formula units is denoted as n_i.

Theoretical values of the MAC (cm) were acquired from the XCOM database [31].

The LAC (μ (cm^{-1})) quantifies the rate of photon absorption per unit thickness. This is determined by multiplying the mass attenuation coefficient by the specific gravity of the substance and is derived by multiplying the MAC by the material's specific gravity, as outlined below [32];

$$\mu = \mu_m \rho \tag{4}$$

where μ_m represents the mass attenuation coefficient of the material and ρ denotes the density of the substance. The MFP (cm) is a crucial metric that indicates radiation attenuation. The MFP in physics refers to the average distance a moving particle (such as an atom, molecule, or photon) travels before substantially changing its direction, energy, or other attributes in a certain setting. This typically results from one or more subsequent collisions with other particles. The mean free path values are determined using the subsequent equation: [33];

$$MFP = (1/\mu) \tag{5}$$

The substance retains residual energy following the establishment of atomic binding energy or secondary photons. The thickness of a material, referred to as the HVL (cm), functions to diminish photon intensity and assess its capacity to attenuate gamma rays. The half-value layer (HVL), or half-value thickness, is the thickness at which the intensity of radiation passing through a material is reduced by fifty percent. The subsequent calculation is employed to ascertain the HVL [33];

$$HVL = ln\ 2/\mu \tag{6}$$

TVL, or the tenth-value layer, is a comparable concept. The entire amount of material necessary to attenuate 90% of the radiation, so reducing it to one-tenth of its original intensity, is referred to as the TVL, as indicated in equation (5) [33];

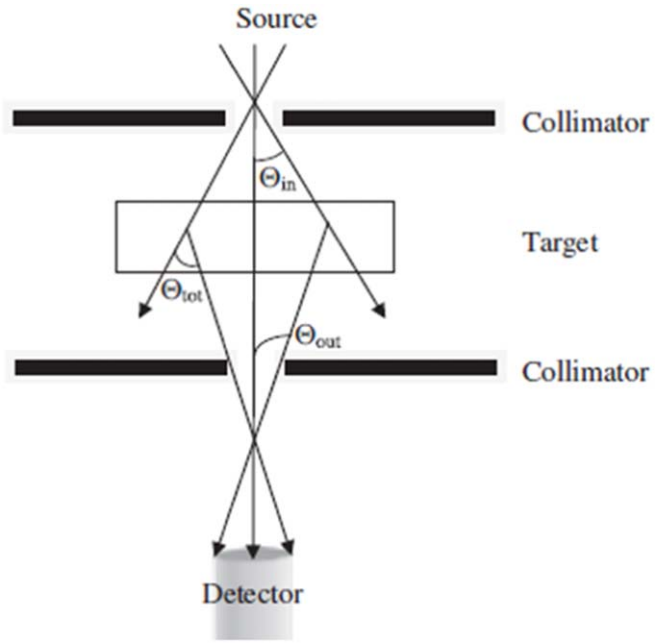

Figure 2. Ray-diagram representation.

$$TVL = ln10/\mu \tag{7}$$

where μ is the total LAC.

This technique facilitates the calculation of gamma-ray absorption parameters of CeO_2 thin films of six different molarities by using narrow-beam x-ray transmission geometry to measure different gamma energies. Figure 1 illustrates the experimental configuration, comprising the secondary source, primary source americium-241 (Am-241), absorber, and detection system. The Am-241radioactive annular source was selected because to its compatibility with secondary targets, ability to facilitate non-destructive excitation, independence from a power source, and capacity to generate an adequate quantity of gamma rays. The secondary source beam impacts the Am target, while the absorber captures the emitted beam from the Am-241 target.

Lead collimators around the detector to obstruct radiation from adjacent objects from accessing it. Three collimators with apertures of 1.2, 1.2, and 1 mm were placed at distances of 30, 75, and 120 mm from the secondary source, respectively. The width of each collimator measured 5 mm. The samples were placed on a specimen holder, 70 mm from the secondary source. The separation between the secondary source and the detector is 135 mm [34]. Figure 2 illustrates the total scatter acceptance angle (θ_{tot}), defined as the sum of the angle encompassed by the exit collimation (θ_{out}) and the angle represented by the incident beam divergence (θ_{in}).

3. Result and discussion

XRD measurements were carried out in the range of 25° to 50° to perform the structure analysis of thin films produced at different molarities. As seen in figure 3(a), three peaks belonging to CeO_2 thin films were observed and the main peak was determined to be in the (111) plane at 28.33°. It was observed that the peaks of CeO_2 thin films were consistent with the literature and the peak intensity increased as the thin film thickness increased [35, 36]. Considering that D is the crystal size, λ is the x-ray wavelength, θ is the Bragg angle, and β is the half-peak width, the average crystal size of thin films can be easily calculated by the Debye–Scherrer equation (equation (8)) based on the x-ray diffraction patterns [37, 38].

$$\mathrm{D} = 0.9\lambda/\beta \cos\theta \tag{8}$$

The crystal size results calculated by taking into account the (111) plane, which is the main peak of CeO_2 thin films, are given in figure 3(b). According to the results obtained, the average crystal size increases with increasing molarity [39].

In figure 3(b), the average crystal size values of thin films prepared at five different molarities are presented. Since no CeO_2 peak was observed in the 0.05 M solution, the crystal size could not be calculated. However, the crystal size of the thin film obtained from the 0.1 M solution was calculated as 5.80 nm. For the 0.2 M, 0.3 M, 0.4 M, and 0.5 M solutions, the crystal sizes were determined to be 7.40 nm, 9.10 nm, 10.40 nm, and 10.10 nm,

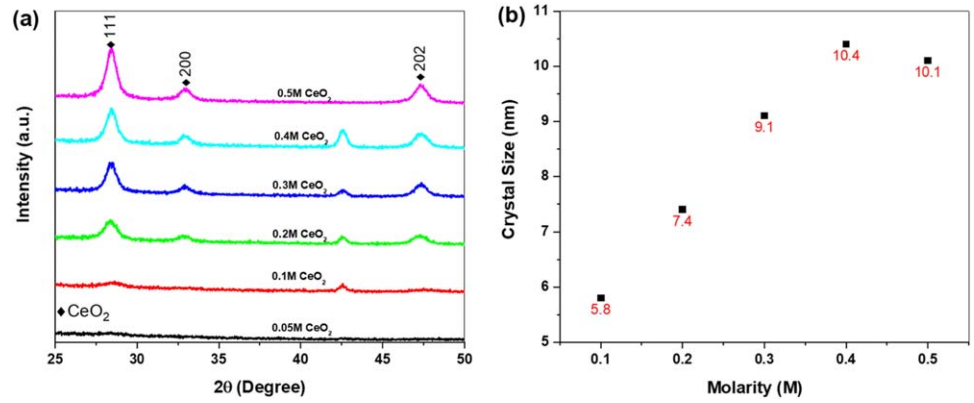

Figure 3. XRD patterns (a) And crystal size (b) of different molarities CeO_2 thin films.

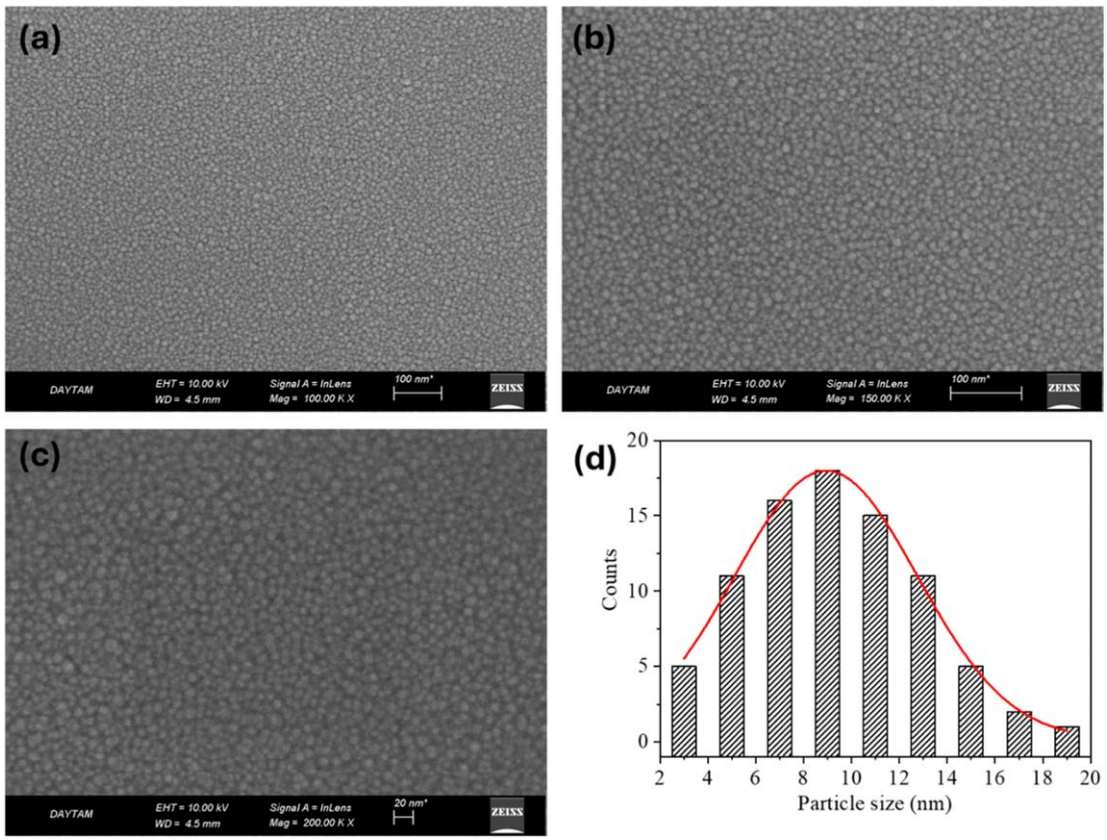

Figure 4. FESEM images of 0.3 M CeO_2 thin films captured at various magnifications.

respectively. The average crystal size for the (111) plane of the thin films prepared at these five molarities was calculated as 8.56 nm, which is consistent with the literature [40]. Figure 4 shows the results of FESEM investigations at various magnifications to investigate the surface morphology of 0.3M CeO_2 thin films. The obtained results show that the CeO_2 thin film has a granular structure and is uniformly dispersed over the surface of the crystalline silicon. FESEM pictures, in addition to XRD investigations, verify the homogenous film production and the structure of CeO_2 thin films. The particle size was determined from image analysis of FE-SEM observations in conjunction with ImageJ software. Histogram plot of the samples prepared at 0.3 M CeO_2 thin films is shown figure 4(d). The particle sizes of CeO_2 thin films were calculated as 8.93 nm, which is seen to be in good agreement with the value obtained from XRD measurements.

Also, The thickness values corresponding to each molarity for thin films prepared at different molarities are presented in figure 5. The thickness values were calculated theoretically by fitting the reflectance curves in previous study [41] and using the Fresnel equations in equation (9).

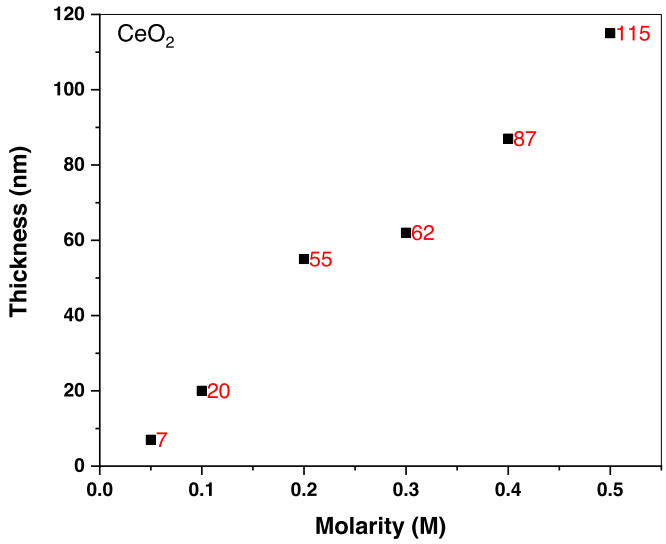

Figure 5. The molarity and thickness values of the CeO_2 thin films.

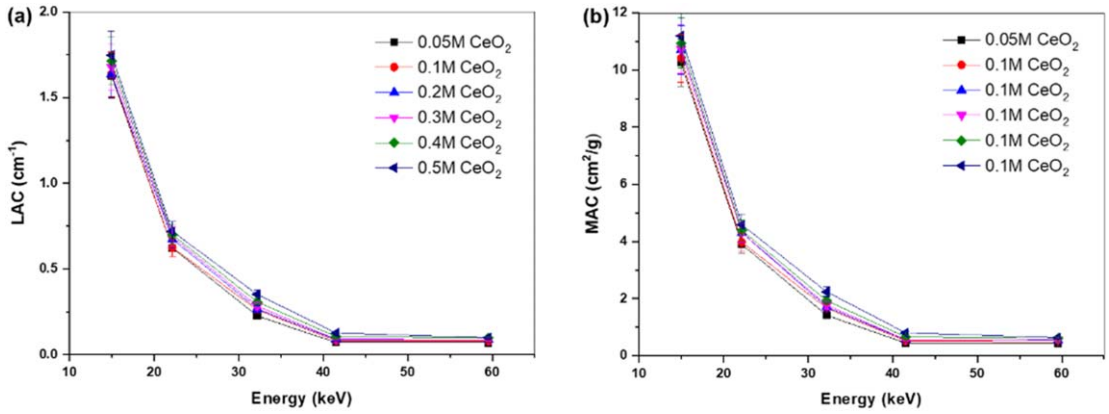

Figure 6. LAC and MAC of CeO_2 thin films at various molarities as a function of energy.

$$R = |r^2| = \frac{r_1^2 + r_2^2 + 2r_1 r_2 \cos 2\theta}{1 + r_1^2 r_2^2 + 2r_1 r_2 \cos 2\theta} \tag{9}$$

where, $r_1 = \frac{n_0 - n_1}{n_0 + n_1}$, $r_2 = \frac{n_1 - n_2}{n_1 + n_2}$, $\theta = \frac{2\pi n_1 d_1}{\lambda}$, d_1 is thin film thickness, n_1 is thin film refractive index, n_0 is the air refractive index, n_2 is substrate refractive index, and θ is light incidence angle [42, 43].

As can be seen from the figure 5, increasing molarity caused an increase in thin film thickness. For example, while the 0.05 M CeO_2 thin films with the lowest molarity had a thickness of 7 nm, a thickness value of around 115 nm was obtained for 0.5M CeO_2 thin films. In the following stages of the study, the thickness values corresponding to each molarity were used to calculate the density of the thin films and experimental calculations were carried out accordingly.

Determination of shielding parameters of thin films is very important in terms of determining the usage areas of the material. In this study, LAC, MAC, TLV, MFP and HVL parameters were determined experimentally as shielding parameters, respectively. Figure 6 and table 1 show the LAC (μ) and MAC (μ/ρ) values of samples with different CeO_2 concentrations at specific energy levels such as 14.957 keV, 22.162 keV, 32.191 keV, 41.529 keV and 59.543 keV. The results in the table reveal that both LAC and MAC values decrease as the energy level increases, but the increase in CeO_2 molarity leads to a strong increase on these coefficients. For example, at 14.957 keV energy, LAC is 2.685 for 0.05 M CeO_2, while this value increases to 7.239 at 0.5 M CeO_2. Similarly, at 0.05 M CeO_2, MAC is 0.213, and at 0.5 M CeO_2, it rises to 0.574. The efficiency of CeO_2 as a radiation attenuating material is demonstrated by the fact that an increase in CeO_2 concentration raises the absorption capacity at

Table 1. Experimental values of LAC and MAC for cerium dioxide thin films at different molarity rate for the different K alpha energies.

		Energy (keV)				
	Samples	14.957	22.162	32.191	41.529	59.543
LAC (cm^{-1})	0.05 M CeO_2	1.627 ± 0.131	0.622 ± 0.050	0.226 ± 0.018	0.070 ± 0.006	0.069 ± 0.006
	0.1 M CeO_2	1.635 ± 0.131	0.625 ± 0.050	0.261 ± 0.021	0.080 ± 0.006	0.078 ± 0.006
	0.2 M CeO_2	1.637 ± 0.134	0.675 ± 0.054	0.267 ± 0.021	0.087 ± 0.007	0.086 ± 0.007
	0.3 M CeO_2	1.677 ± 0.137	0.688 ± 0.055	0.282 ± 0.023	0.090 ± 0.007	0.088 ± 0.007
	0.4 M CeO_2	1.713 ± 0.140	0.700 ± 0.056	0.308 ± 0.025	0.105 ± 0.008	0.097 ± 0.008
	0.5 M CeO_2	1.747 ± 0.141	0.720 ± 0.058	0.351 ± 0.028	0.126 ± 0.010	0.099 ± 0.008
MAC (cm^2/g)	0.05 M CeO_2	10.260 ± 0.821	3.902 ± 0.312	1.417 ± 0.113	0.442 ± 0.035	0.432 ± 0.035
	0.1 M CeO_2	10.415 ± 0.833	3.974 ± 0.318	1.663 ± 0.133	0.512 ± 0.041	0.493 ± 0.039
	0.2 M CeO_2	10.699 ± 0.856	4.309 ± 0.345	1.703 ± 0.136	0.555 ± 0.044	0.547 ± 0.044
	0.3 M CeO_2	10.750 ± 0.860	4.315 ± 0.345	1.770 ± 0.142	0.567 ± 0.045	0.555 ± 0.044
	0.4 M CeO_2	10.942 ± 0.875	4.385 ± 0.351	1.927 ± 0.154	0.656 ± 0.052	0.609 ± 0.049
	0.5 M CeO_2	11.200 ± 0.896	4.585 ± 0.367	2.237 ± 0.179	0.801 ± 0.064	0.632 ± 0.051

every energy level [44, 45]. Furthermore, studies have demonstrated that a larger mass attenuation coefficient value is necessary for improved x-ray and gamma-ray shielding efficacy [46].

HVL, MFP and TVL values, which are another important radiation shielding parameters, were obtained for five different radiation energy levels from 14.957 KeV to 59.543 KeV for six different molarities and are presented in table 2. Additionally, graphs of these values are given in figures 7(a)–(c). HVL is defined as the thickness of the material at which the intensity of the incoming radiation is reduced by half and TVL is defined as the thickness of the material at which the intensity of the incoming radiation is reduced by one-tenth. MFP is the average distance that radiation can travel in a substance before any two successive collisions [47]. When figure 7(a) was examined, it was seen that the HVL values increased significantly with increasing energy. For example, for 0.05 M, the HVL value was 0.42 cm at the lowest energy of 14.957 keV, while it reached approximately 10 cm at the highest energy of 59.543 keV. This shows that higher energy radiation can penetrate deeper into the material [48, 49]. In addition, as can be seen from table 2, it was determined that there was a decrease in HVL values with the increase in molarity in each energy. It was observed that with the increase in molarity at 14.957 keV energy, the HVL value decreased from 0.424 cm to 0.394 cm, while at 22.162 keV energy, from 1.11 cm to 0.96 cm, at 32.191 keV energy, from 3.07 cm to 1.97 cm, at 41.539 keV energy, from 9.85 cm to 5.51 cm and finally at 59.543 keV energy it decreased from 10.06 cm to 6.98 cm. These results clearly show that higher concentrations of CeO_2 increase the absorption of radiation [44]. However, the results indicate that high-energy radiation penetrates less dependent on material thickness [50]. Similarly, when the MFP values given in figure 7(b) were examined depending on the radiation energy and CeO_2 molarity, distinct trends affecting the material-radiation interactions were observed. When the radiation energy sent to the material was increased from 14.957 keV to 59.543 keV, it was observed that the MFP values increased steadily from 0.61 cm to 14.51 cm (0.05 M CeO_2) This is attributed to the higher energy radiation traveling longer distances [51]. However, with the increase in CeO_2 molarity, more radiation was absorbed or scattered for all energies, and thus a decrease in MFP values was observed.

Herein, the lowest MFP values were observed at the low energy level of 14.957 keV and the highest molarity value (0.5 M), revealing the dominance of absorption mechanisms in a dense environment. In contrast, the highest MFP values were obtained in high energy (59.543 keV) and low molarity (0.05 M) samples because radiation-material interactions were determined to be at a minimum level in these conditions. In figure 7(c), TVL values are presented depending on the radiation energy and CeO_2 molarity. The increase in the energy level from 14.957 keV to 59.543 keV decreased the possibility of radiation interacting with the material, which caused the TVL values to increase. This shows that high energy photons travel longer distances in the material without being weakened. On the other hand, the increase in CeO_2 molarity increased the density of the material, causing the radiation to interact more frequently and decreasing the TVL values. The lowest TVL values indicate that low energy radiation (14.957 keV) is rapidly absorbed in a high density (0.5 M) medium and an effective attenuation occurs. In contrast, a high energy (59.543 keV) and low density (0.05 M) medium produced the highest TVL values of 33.423 cm, allowing the radiation to pass through the material with minimal interaction.

Calculations and measurements were carried out by considering the margins of error given in table 3. From the results, it can be concluded that CeO_2 thin films at higher molarities provide better radiation absorption properties and thus may be potential candidates for radiation shielding applications.

Table 2. Experimental values of MFP, HVL, TVL for cerium dioxide thin films at different molarity rate for different K alpha energies.

Samples	Energy (keV)								
	14.957			22.162			32.191		
	MFP	HVL	TVL	MFP	HVL	TVL	MFP	HVL	TVL
0.05 M CeO_2	0.612 ± 0.049	0.424 ± 0.034	1.408 ± 0.113	1.608 ± 0.129	1.114 ± 0.089	3.702 ± 0.296	4.429 ± 0.354	3.070 ± 0.246	10.197 ± 0.816
0.1 M CeO_2	0.611 ± 0.049	0.423 ± 0.034	1.407 ± 0.113	1.601 ± 0.128	1.110 ± 0.089	3.687 ± 0.295	3.825 ± 0.306	2.651 ± 0.212	8.808 ± 0.705
0.2 M CeO_2	0.596 ± 0.048	0.413 ± 0.033	1.373 ± 0.110	1.481 ± 0.118	1.026 ± 0.082	3.409 ± 0.273	3.746 ± 0.300	2.596 ± 0.208	8.625 ± 0.690
0.3 M CeO_2	0.584 ± 0.047	0.405 ± 0.032	1.344 ± 0.108	1.454 ± 0.116	1.008 ± 0.081	3.348 ± 0.268	3.545 ± 0.284	2.457 ± 0.197	8.163 ± 0.653
0.4 M CeO_2	0.572 ± 0.046	0.397 ± 0.032	1.318 ± 0.105	1.428 ± 0.114	0.990 ± 0.079	3.289 ± 0.263	3.250 ± 0.260	2.253 ± 0.180	7.484 ± 0.599
0.5 M CeO_2	0.569 ± 0.045	0.394 ± 0.032	1.309 ± 0.105	1.389 ± 0.111	0.963 ± 0.077	3.198 ± 0.256	2.847 ± 0.228	1.973 ± 0.158	6.554 ± 0.524

Samples	Energy (keV)					
	41.529			59.543		
	MFP	HVL	TVL	MFP	HVL	TVL
0.05 M CeO_2	14.211 ± 1.137	9.850 ± 0.788	32.721 ± 2.618	14.515 ± 1.161	10.061 ± 0.805	33.423 ± 2.674
0.1 M CeO_2	12.432 ± 0.995	8.617 ± 0.689	28.626 ± 2.290	12.902 ± 1.032	8.943 ± 0.715	29.709 ± 2.377
0.2 M CeO_2	11.488 ± 0.919	7.963 ± 0.637	26.453 ± 2.116	11.654 ± 0.932	8.078 ± 0.646	26.835 ± 2.147
0.3 M CeO_2	11.065 ± 0.885	7.669 ± 0.614	25.477 ± 2.038	11.311 ± 0.905	7.840 ± 0.627	26.045 ± 2.084
0.4 M CeO_2	9.552 ± 0.764	6.621 ± 0.530	21.994 ± 1.760	10.289 ± 0.823	7.132 ± 0.571	23.692 ± 1.895
0.5 M CeO_2	7.953 ± 0.636	5.512 ± 0.441	18.312 ± 1.465	10.077 ± 0.806	6.985 ± 0.559	23.204 ± 1.856

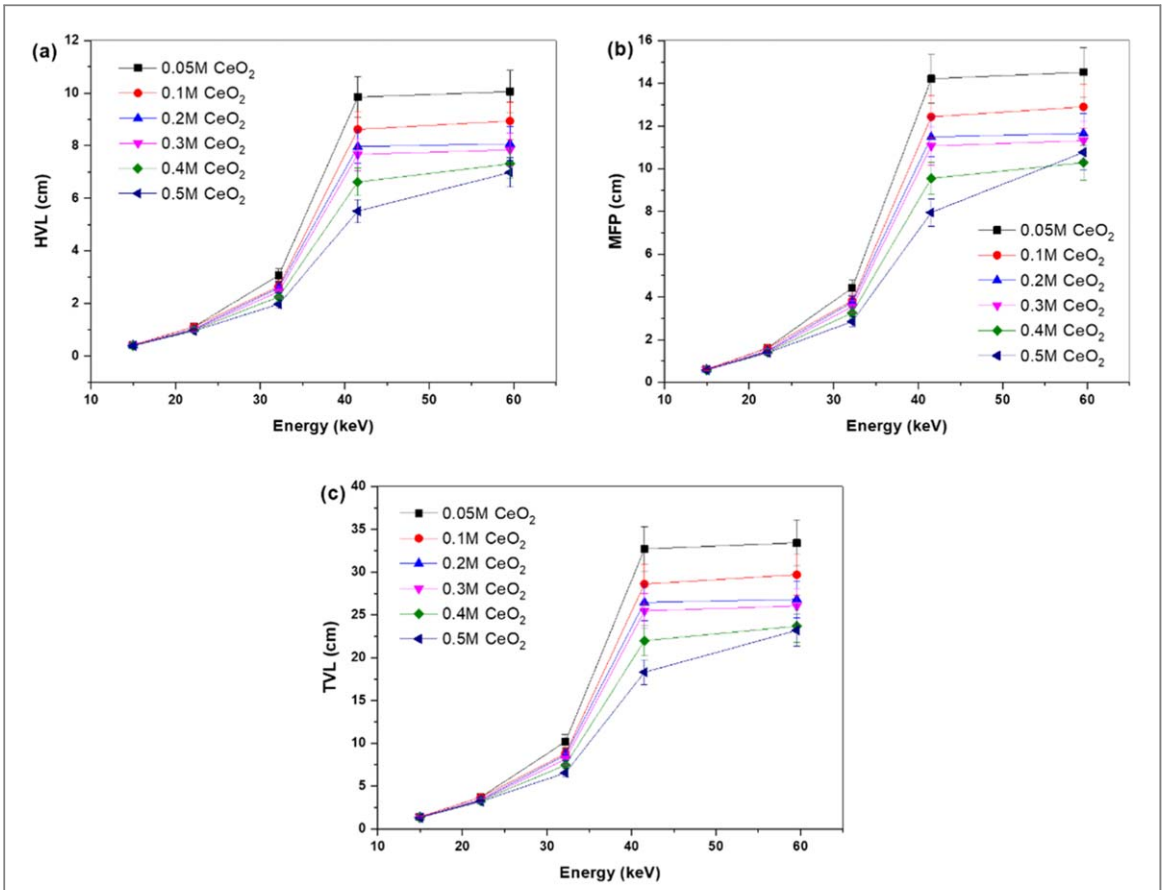

Figure 7. HVL, MFP and TVL of CeO_2 thin films at various molarities as a function of energy.

Table 3. Margins of error in calculating parameters.

Nature of uncertainty	Uncertainty [%]
The original and attenuated photon intensity	⩽5
Photon detection statistics	⩽3
Specimen thickness	⩽2

4. Conclusions

In this study, the structural, morphological and radiation shielding properties of CeO_2 thin films prepared at different molarities were investigated. XRD pattern analyses showed that the crystal structure of the films was consistent with the literature and that the crystal sizes increased with the increase in molarity. FESEM images revealed that the films were spread homogeneously on the surface and had a granular structure. The thickness of the thin films increased with molarity and this increase contributed positively to the radiation shielding parameters of the films. In particular, it was observed that LAC and MAC values increased with molarity, while HVL, MFP and TVL values decreased. This has proved that CeO_2 thin films can effectively absorb low-energy radiation and exhibit better radiation shielding performance at high molarities. As a result, CeO_2 thin films can be considered as a potential material for radiation protection applications.

CRediT authorship contribution statement

Imran Kanmaz: Conceptualization, Methodology, Validation, Investigation, Visualization, and Writing–Review, Editing and Finalizing, **Oğuzkağan Köksal:** Calculations. **Erhan Cengiz:** Supervision. **Gökhan Apaydın:** Supervision. **Murat Tomakin:** Supervision. All authors discussed experiments and results, have reviewed and edited the manuscript. All authors have given approval for the final version of the manuscript.

Acknowledgments

This research was supported by The Scientific and Technological Research Council of Türkiye (TUBITAK) under project number 121C375. We thank TUBITAK for its support.

Data availability statement

All data that support the findings of this study are included within the article (and any supplementary files).

ORCID iDs

İmran Kanmaz https://orcid.org/0000-0001-8827-1590
Oğuz Kağan Köksal https://orcid.org/0000-0003-2671-6683
Gökhan Apaydin https://orcid.org/0000-0002-4647-344X
Murat Tomakin https://orcid.org/0000-0003-1887-848X
Erhan Cengiz https://orcid.org/0000-0002-4094-5784

References

[1] Arif Sazali M, Alang Md Rashid N K and Hamzah K 2019 A review on multilayer radiation shielding *Materials Science and Engineering* **555** 012008 IOP Conference Series: Materials Science and EngineeringIOP Publishing
[2] Kim B *et al* 2010 Intrinsic electromagnetic radiation shielding/absorbing characteristics of polyaniline-coated transparent thin films *Synth. Met.* **160** 1838–42
[3] Henaish A *et al* 2021 Characterization of optical and radiation shielding behaviors of ferric oxide reinforced bismuth borate glass *Phys. Scr.* **96** 075801
[4] Badawy S M and Abd El-Latif A 2017 Synthesis and characterizations of magnetite nanocomposite films for radiation shielding *Polym. Compos.* **38** 974–80
[5] AbuAlRoos N J, Amin N A B and Zainon R 2019 Conventional and new lead-free radiation shielding materials for radiation protection in nuclear medicine: a review *Radiat. Phys. Chem.* **165** 108439
[6] El Sayed A M 2018 Modification of the micro-structural and optical properties of nanoparticulate Pb-doped magnesia thin films *Mater. Res. Express* **5** 116403
[7] Mohaseba M A and Aboud A A 2023 Effect of Pb doping onto physical properties of ZnO thin films deposited by AACVD *J. Mater. Sci., Mater. Electron.* **34** 941
[8] Elidrissi B *et al* 2000 Structural and optical properties of CeO_2 thin films prepared by spray pyrolysis *Thin Solid Films* **379** 23–7
[9] Zimou J *et al* 2021 Structural, morphological, optical, and electrochemical properties of Co-doped CeO_2 thin films *Mater. Sci. Semicond. Process.* **135** 106049
[10] Anandan C and Bera P 2013 XPS studies on the interaction of CeO_2 with silicon in magnetron sputtered CeO_2 thin films on Si and Si3N4 substrates *Appl. Surf. Sci.* **283** 297–303
[11] Shaaban K S *et al* 2024 Role of CeO_2 in the enhancement of the properties of the SiO_2-B_2O_3-BaO-Li_2O-glass system: structural, mechanical and radiation shielding study *Materials Today Communications* **38** 108309
[12] Li Y *et al* 2017 The protection of CeO_2 thin film on Cu-SAPO-18 catalyst for highly stable catalytic NH3-SCR performance *Chem. Eng. J.* **330** 926–35
[13] Stefanov P *et al* 2004 Electrochemical deposition of CeO_2 on ZrO_2 and Al_2O_3 thin films formed on stainless steel *Surf. Coat. Technol.* **180** 446–9
[14] Debnath S, Islam M and Khan M 2007 Optical properties of CeO_2 thin films *Bull. Mater. Sci.* **30** 315–9
[15] Patil B and Pawar S 2011 Structural, morphological and electrical properties of spray deposited nano-crystalline CeO_2 thin films *J. Alloys Compd.* **509** 414–20
[16] Beie H-J and Gnörich A 1991 Oxygen gas sensors based on CeO_2 thick and thin films *Sensors Actuators* B **4** 393–9
[17] Rajendran P, Muthuraj A and Rajagounder N E 2022 Review on CeO_2-based corrosion coatings *Transactions of the Indian Ceramic Society* **81** 158–74
[18] Zhang S *et al* 2010 Preparation and corrosion resistance studies of nanometric sol–gel-based CeO_2 film with a chromium-free pretreatment on AZ91D magnesium alloy *Electrochim. Acta* **55** 870–7
[19] Yamashita M *et al* 2002 Synthesis and microstructure of calcia doped ceria as UV filters *J. Mater. Sci.* **37** 683–7
[20] Alonzo-Medina G *et al* 2013 Understanding the thermal annealing process on metallic thin films *Materials Science and Engineering* **45** 012013 IOP Conference Series: Materials Science and EngineeringIOP Publishing
[21] Mahmood A *et al* 2010 Effect of thermal annealing on the structural and optical properties of ZnO thin films deposited by the reactive e-beam evaporation technique *Phys. Scr.* **82** 065801
[22] Akgul F A *et al* 2014 Influence of thermal annealing on microstructural, morphological, optical properties and surface electronic structure of copper oxide thin films *Mater. Chem. Phys.* **147** 987–95
[23] Yin Z *et al* 2019 Characterization and application of PVDF and its copolymer films prepared by spin-coating and Langmuir–Blodgett method *Polymers* **11** 2033
[24] Kanmaz I, Mandong A M and Uzum A 2020 Solution-based hafnium oxide thin films as potential antireflection coating for silicon solar cells *J. Mater. Sci., Mater. Electron.* **31** 21279–87
[25] Apaydın G *et al* 2009 Studies on mass attenuation coefficients, effective atomic numbers and electron densities for CoCuAg alloy thin film *Phys. Scr.* **79** 055302
[26] Koksal O *et al* 2019 Assessment of the mass attenuation parameters with using gamma-rays for manganese substituted nano hydroxyapatite *Radiat. Phys. Chem.* **159** 76–80

[27] Koksal O et al 2022 The effect of metal rate on the gamma shielding parameters of hydroxyapatite at medical treatment energies Appl. Radiat. Isot. 190 110456
[28] Kavaz E et al 2020 Gamma ray shielding effectiveness of the Portland cement pastes doped with brass-copper: an experimental study Radiat. Phys. Chem. 166 108526
[29] Sayyed M I et al 2019 Evaluation of radiation absorption capacity of some soil samples Radiochim. Acta 107 83–93
[30] Abouhaswa A and Kavaz E 2020 Bi_2O_3 effect on physical, optical, structural and radiation safety characteristics of $B_2O_3Na_2O$-ZnOCaO glass system J. Non-Cryst. Solids 535 119993
[31] Berger M J et al 1999 XCOM: photon cross section database (version 1.2) (http://physics.nist.gov/xcom)
[32] Sayyed M et al 2022 Theoretical investigation of the radiation-protection properties of the CBS glass family Optik 258 168851
[33] Singh K et al 2015 Gamma radiation shielding analysis of lead-flyash concretes Appl. Radiat. Isot. 95 174–9
[34] Cengiz E, Dogan M and Koksal O K 2013 LIII subshell absorption jump ratio and jump factor of tantalum Radiat. Phys. Chem. 85 8–11
[35] Channei D et al 2013 Cerium dioxide thin films using spin coating Journal of Chemistry 2013 1–4
[36] Gatea H A and Hachim F 2023 Impact of molarity on the structural, morphological and optical properties of CeO_2 thin films prepared by spray pyrolysis technique Int. J. Thin. Fil. Sci. Tec 12 53–7
[37] Fatimah S et al 2022 How to calculate crystallite size from x-ray diffraction (XRD) using scherrer method ASEAN Journal of Science and Engineering 2 65–76
[38] Senol S et al 2014 Effect of annealing time on the structural, optical and electrical characteristics of DC sputtered ITO thin films J. Mater. Sci., Mater. Electron. 25 4992–9
[39] Johnson J , S et al 2017 A facile route to synthesis of hexagonal shaped CeO_2 nanoparticles J. Mater. Sci., Mater. Electron. 28 3740–5
[40] Zimou J et al 2022 Influence of manganese rate on structural, optical and electrochemical properties of CeO_2 thin films deposited by spray pyrolysis: Supercapacitor applications J. Rare Earths 40 1611–8
[41] Kanmaz İ and Tomakin M 2023 Anti-reflective effect of CeO_2 thin films produced by sol-gel method on crystalline silicon solar cells J. Sol-Gel Sci. Technol. 108 361–7
[42] Sharma R, Amit G and Ajit V 2017 Effect of single and double layer antireflection coating to enhance photovoltaic efficiency of silicon solar Journal of Nano- and Electronic Physics 9 02001
[43] KANMAZ İ 2023 Simulation of CdS/p-Si/p+-Si and ZnO/CdS/p-Si/p+-Si heterojunction solar cells Results in Optics 10 100353
[44] Kaewjaeng S et al 2022 X-ray radiation shielding of CeO_2 doped borosilicate glasses and their luminescence characteristics Radiat. Phys. Chem. 191 109825
[45] Alharshan G A et al 2024 CeO_2 additive to bismo-borate glasses: synthesis, structure, physical characteristics, and radiation protection competence J. Mater. Sci., Mater. Electron. 35 862
[46] Kaur S and Singh K 2014 Investigation of lead borate glasses doped with aluminium oxide as gamma ray shielding materials Ann. Nucl. Energy 63 350–4
[47] Alwany A B et al 2022 Structural, optical and radiation shielding properties of ZnS nanoparticles QDs Optik 260 169124
[48] Buzok E B et al 2024 The structural, optical, electrical and radiation shielding properties of Co-doped ZnO thin films Radiat. Phys. Chem. 222 111840
[49] Soğuksu A K et al 2024 Synthesis and characterizations of Ce-doped ZnO thin films for radiation shielding Opt. Mater. 148 114941
[50] Al-Saleh W M et al 2023 Comprehensive study of the radiation shielding feature of polyester polymers impregnated with iron filings e-Polymers 23 20230096
[51] Aygün B 2021 Neutron and gamma radiation shielding Ni based new type super alloys development and production by Monte Carlo Simulation technique Radiat. Phys. Chem. 188 109630